Available online at www.sciencedirect.com
ScienceDirect
Journal of Power Sources 162 (2006) 480–485
JOURNAL OF POWER SOURCES
www.elsevier.com/locate/jpowsour

Short communication

A study on sintering aids for $Sm_{0.2}Ce_{0.8}O_{1.9}$ electrolyte

Xinge Zhang *, Cyrille Decès-Petit, Sing Yick, Mark Robertson, Olivera Kesler, Radenka Maric, Dave Ghosh

Institute for Fuel Cell Innovation, National Research Council Canada, 3250 East Mall, Vancouver, BC, Canada V6T 1W5

Received 30 May 2006; received in revised form 21 June 2006; accepted 22 June 2006
Available online 22 August 2006

Abstract

In this study, an addition of Co oxide or Cu oxide to $Sm_{0.2}Ce_{0.8}O_{1.9}$ (SDC) was studied to improve the sinterability of SDC. It has been found that both Co and Cu oxide are very effective as sintering aids, and the SDC sintering temperature can be reduced from 1400 °C without aids to below 1000 °C with only 1 at.% of either Cu oxide or Co oxide. As compared to the pure SDC, a slight decrease of ionic conductivity was observed in SDC with Cu sintering aid. There is no obvious effect on electrochemical property of SDC with Co sintering aid under 2.5 at.%.

Keywords: SDC electrolyte; SOFC; Sintering aids; Cobalt oxide; Copper oxide

1. Introduction

Ceria-based ceramic materials doped with Sm and/or Gd have been acknowledged to be the most promising electrolytes for solid oxide fuel cells operating below 600 °C due to their high ionic conductivity and good compatibility with electrodes, especially with high performing Co-content cathodes. Maximum power density of anode supported thin ceria-based electrolyte cells has been reported over 880 mW cm^{-2} at 600 °C with H_2 fuel [1,2]. However, the ceria electrolytes are difficult to densify below 1400 °C [3–6]. If a dense ceria-based electrolyte can be prepared at lower temperatures it can be co-sintered with the electrode components, which simplifies the fabrication process and reduces the cost, helping with porous electrode microstructure control and avoiding phase diffusion and chemical interaction problems.

In order to sinter doped ceria materials at a lower temperature, several methods have proven effective, which could be classified into two categories:

1) Using ultra-fine powders at submicron and nanometer size by special synthesis, such as hydrothermal synthesis [7,8], oxalate co-precipitation [9,10], chemical combustion vapour synthesis [11,12] or intensive mechanical milling [13]; the decrease of a starting particle size enables the densification at a lower heating temperature because of the increased driving force (specific surface area) of sintering. However, a small pore size between ultra-fine particles produces a high capillary force in the powder compact which is the origin of low packing density and cracks formed during drying and firing [14,15].
2) Adding a sintering promoter or aid in a limited amount [3,13]. It has been reported that Mn_2O_3 and Co_3O_4 promotes grain growth of doped ceria even at initial stages of sintering, while Ga_2O_3 promoted rearrangement of particles. The sintering temperature could be decreased from 1600 to 1400 °C by adding 1 at.% of such aids [3].

In this paper, we studied the influence of Co and Cu oxides as sintering aids on sintering behavior, conductivity, phase and microstructure of SDC.

2. Experimental

2.1. Sample preparation

Table 1 lists the starting chemicals and ceramic powder materials used in this study. Firstly, both Co and Cu nitrates were separately dissolved in ethanol at 1.0, 2.5 and 5.0 at.%, through

* Corresponding author. Tel.: +1 604 221 3077; fax: +1 604 221 3088.
E-mail address: xinge.zhang@nrc.gc.ca (X. Zhang).

0378-7753/$ – see front matter © 2006 Elsevier B.V. All rights reserved.
doi:10.1016/j.jpowsour.2006.06.061

Table 1
Properties and supplier of starting materials

Material	Composition	Properties	Supplier
Co additive	$Co(NO_3)_2{\cdot}6H_2O$	Formula weight (FW) 291.04	Alpha Aesar, Lot#23282
Cu additive	$Cu(NO_3)_2{\cdot}3H_2O$	FW 241.60	Alpha Aesar, Lot#K10N42
Electrolyte	$Sm_{0.2}Ce_{0.8}O_{1.9}$ (SDC)	FW 172.6; D50: 0.40 μm; surface area: 7.0 $m^2\ g^{-1}$	Praxair Lot#03-P4687DM
Cathode	$Sm_{0.5}Sr_{0.5}CoO_3$ (SSCo)	D50: 0.80 μm; surface area: 5.16 $m^2\ g^{-1}$	Praxair
Anode	NiO type F + SDC	D50: 1.0 μm; surface area: 4.0 $m^2\ g^{-1}$	Novamet (SDC from Praxair)

a ball milling process, using nalgene bottles with Ø 5 mm YSZ balls, before adding SDC powder. After adding SDC powder, ball milling was carried out for 40 h, with subsequent drying at 50 °C for 8 h and separation of powders for thermal decomposition at 500 °C for 5 h in air. The obtained seven types of powders, including one blank SDC powder (without Co or Cu additive), were pressed at 40–50 MPa into pillars of Ø 5 mm about 10 mm length and pellets of Ø 20 mm about 2.0 mm thick. The pillar samples were used for shrinkage-sintering studies using a Setsys 16/18 TMA (Setaram). The sintered pellet samples after surface polishing were used for XRD analysis and electrochemical characterization. Both NiO–SDC anode and $Sm_{0.5}Sr_{0.5}CoO_3$ cathode were applied on the polished samples and co-sintered at 1000 °C for 2 h in air. Measurements were performed in fuel cell operating conditions, i.e., at 600 °C with 97% H_2 + 3% H_2O as anode gas and air as cathode gas, both at flow rates of 100 ml min^{-1}. Cyclic voltammetry curves were measured using a Solartron 1480 at a scan rate of 0.5 mV s^{-1}.

2.2. Sample characterization

Powder characterization was performed using a Mastersizer 2000 (Malvern Instruments Ltd., UK) for particle size analysis and by using a SA3100 Surface Area Analyzer (Beckman Coulter™) for surface area analysis. The density of experimental pellets was measured by Archimedes' method at room temperature.

Table 2
Composition, particle size and surface area of powders and sintering temperature, density and grain size of samples used in this study

Powder composition	Appearance	Mean particle size[a] (μm)	BET surface area ($m^2\ g^{-1}$)
blank-SDC	Yellow	0.18	7.15
5.0 at.%Co-SDC	Green	0.17	8.25
5.0 at.%Cu-SDC	Dark green	0.17	8.39

Sample	T_s (°C) (for 5 h)	Density (g cm^{-3})	Grain size (μm)
blank-SDC	1400	6.948	1–2
1.0 at.% Co	1000	6.865	0.5–1
2.5 at.% Co	1000	6.750	0.5–1
5.0 at.% Co	1000	6.633	0.5–1
1.0 at.% Cu	1000	7.004	SDC: 0.5–1
2.5 at.% Cu	1000	7.009	Cu-compound[b]
5.0 at.% Cu	1000	6.981	>10 μm

[a] Water as dispersant, 4 min ultrasonic agitation.
[b] New phase appeared on the pellet surface with Cu sintering aids, named Cu-compound.

Table 2 gives the composition, particle size and surface area of powders, and sintering temperature, density and grain size of samples in this study. It can be seen that there is a slight increase of the BET surface area of SDC with sintering aids after the powder processing. The increase of BET surface area of SDC after Cu or Co addition and pre-treatment at 500 °C indicated the formation of fine Co or Cu oxides on the SDC particle surface. The density of experimental pellets slightly decreased with the increase of aids content; over 93% theoretical density of the SDC was reached.

3. Results and discussion

3.1. Powder pre-treatment condition

Thermal decomposition of SDC powders with 5 at.% $Co(NO_3)_3{\cdot}6H_2O$ or $Cu(NO_3)_2{\cdot}3H_2O$ was analysed from room temperature to 800 °C in air flowing at 20 ml min^{-1} by TGA and DTA. As shown in Figs. 1 and 2, both Co and Cu nitrates are fully decomposed before 300 °C and the fastest decomposition rate happens at 231 °C for $Co(NO_3)_3$ and 251 °C for $Cu(NO_3)_2$. The DTA results also show the different temperatures for desorbing the adsorbed water in each nitrate.

Based on the TGA results, all SDC powders with nitrates at designed content (0, 1, 2.5 and 5 at.% of Co or Cu) were treated for thermal decomposition at 500 °C for 5 h in air.

3.2. XRD results

The lattice constant was determined using a D8-02 X-ray diffractometer (Bruker AXS GmbH) with Cu Kα radiation at room temperature. The spectra were acquired from 2θ angles of

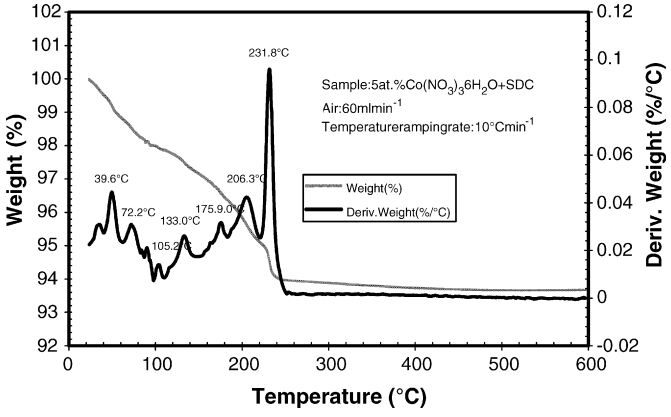

Fig. 1. TGA of SDC powders with 5 at.% $Co(NO_3)_3{\cdot}6H_2O$.

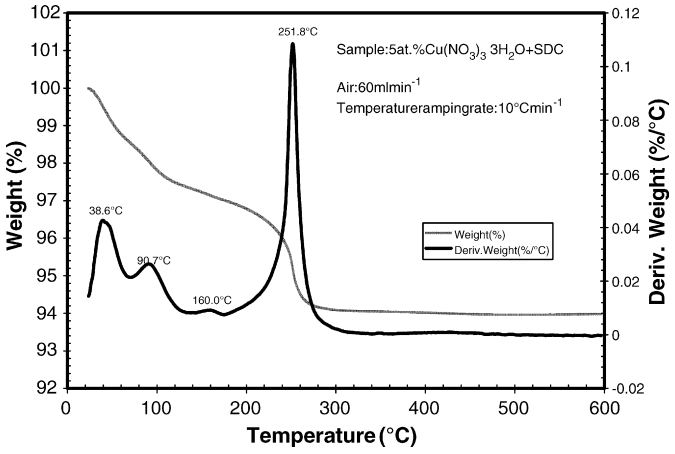

Fig. 2. TGA of SDC powders with 5 at.% $Cu(NO_3)_2{\cdot}3H_2O$.

15° to 85° in steps of 0.02° s^{-1}. All samples were positioned on plasticine using a flat of glass to align the sample in the holder. The results are shown in Fig. 3. It can be seen that no clear impurity phase presents in the XRD patterns of the sample up to 5 at.% Co addition. However, addition of only 1 at.% Cu of the as-fired sample presents CuO (Tenorite) phase at the surface. This CuO phase was removed after polishing the sample surface. As shown in Fig. 4, the SDC lattice parameter shows limited variation with the Co or Cu (polished sample) contents. This may suggest that Co and Cu exist mainly on the SDC grain boundary, and does not enter the SDC lattice. Gauckler and co-workers found the evidence of a grain boundary phase with concentrated Co amount in the $Gd_{0.2}Ce_{0.8}O_{1.9}$ with Co oxide as sintering aid by electron energy loss mapping [16].

3.3. TMA sintering results

The effects of Co or Cu dopant on SDC sintering behaviour are shown in Figs. 5 and 6. It can be seen that the Co or Cu addition shifts the sintering curve towards lower temperature ranges from 1100 for SDC to 800 °C for Co addition and 750 °C for Cu addition, significantly promoting the densification. It was found that increasing dopant amounts from 1 to 5 at.% had a

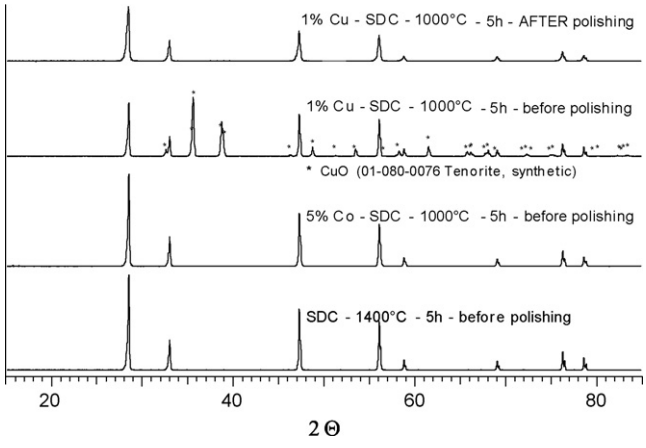

Fig. 3. XRD patterns of sintered SDC with and without Cu or Co addition.

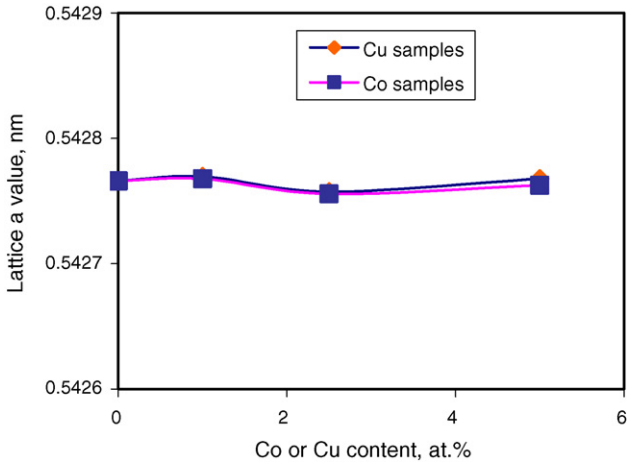

Fig. 4. SDC lattice parameter variation with the Co or Cu (polished sample) content.

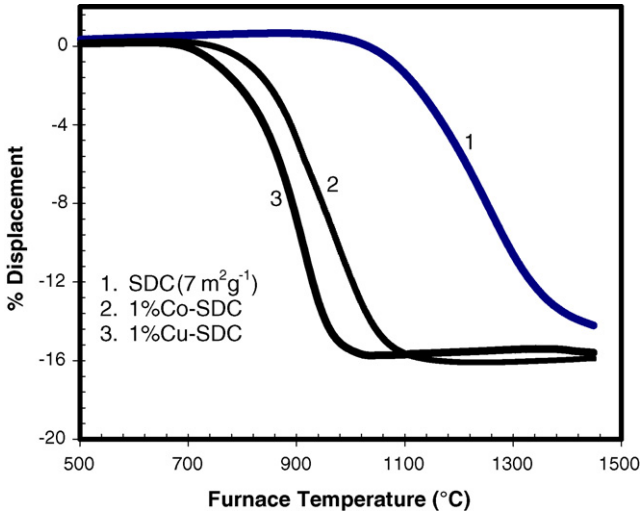

Fig. 5. Linear shrinkage (displacement%) vs. sintering temperature at a heating rate of 5 °C min^{-1}.

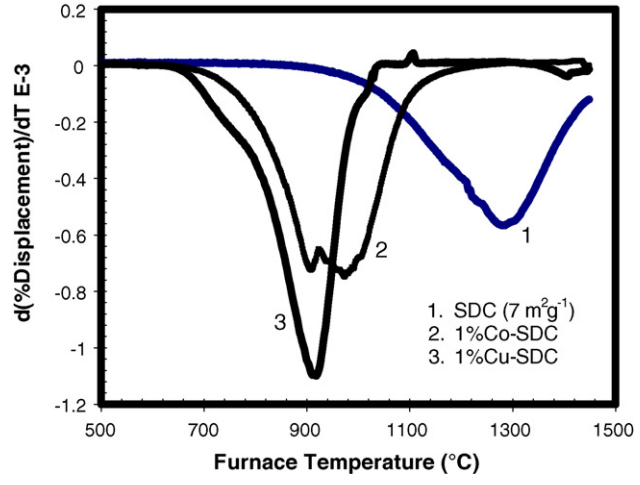

Fig. 6. Linear shrinkage rate vs. sintering temperature at a heating rate of 5 °C min^{-1}.

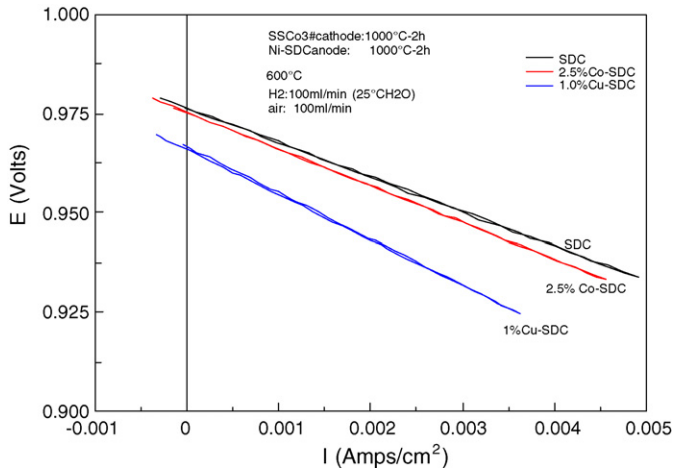

Fig. 7. Cyclic voltammetry curves at 600 °C of three SDC electrolyte cells.

limited effect on the densification behaviour for both Co and Cu addition. Fig. 6 shows the linear shrinkage rate as a function of temperature. This figure clearly shows that the maximum shrinkage rate (S_{max}, $°C^{-1}$) changes with the type of dopant, which is in the following order 0.58 $°C^{-1}$ at 1290 °C for SDC, 0.70–0.72 $°C^{-1}$ at 913–975 °C for Co-SDC and 1.1 $°C^{-1}$ at 920 °C for Cu-SDC. The difference between the temperatures of the maximum shrinkage rate of SDC and with Cu or Co addition is more than 200 °C. Moreover, the Cu and Co addition enhances greatly the densification rate of SDC. A similar result about Co addition was published by Zhang et al. [13,14]. Of the two oxides, Cu oxide is the most effective sintering aid. The measured sample density in Table 2 supports this result. Both liquid phase sintering and viscous flow sintering processes may contribute to the significant reduction of the sintering temperature with Co or Cu aids.

Table 3
Electrolyte conductivity at 600 °C

Electrolyte	SDC	2.5%Co-SDC	1.0%Cu-SDC
Electrode area (cm^2)	0.3529	0.3649	0.3598
Electrolyte thickness (cm)	0.1934	0.2068	0.1972
OCV (V)	0.976	0.975	0.966
Cell resistance ($\Omega\,cm^2$)	9.199	9.21	11.41
Electrolyte conductivity ($S\,cm^{-1}$)	2.10×10^{-2}	2.24×10^{-2}	1.73×10^{-2}

3.4. Electrochemical measurements

Fig. 7 shows the cyclic voltammetry curves at 600 °C of three SDC electrolyte cells. The fitting results are listed in Table 3. It can be seen that the conductivity of SDC is about 0.021 $S\,cm^{-1}$, while a slightly higher conductivity for 2.5%Co-SDC and a little lower conductivity for 1%Cu-SDC. The measured OCV at 600 °C also shows that the addition of Co or Cu to SDC will cause a slight decrease in OCV value, indicating an increase of the ratio of electronic to ionic conductivities.

3.5. SEM analysis

As shown in Fig. 8a, the SDC without sintering aids sintered at 1400 °C for 5 h is dense with the grain size about 1–3 μm. In the case of 1%Co-SDC fired at 1000 °C for 5 h (Fig. 8b), the surface is slightly rough and the starting 1%Co-SDC particle morphology appears on the surface. The measured density is slightly lower than that of SDC (see Table 2).

For 1%Cu-SDC (Fig. 8c) the SDC particles are well sintered at 1000 °C, however, large CuO grains exist at the surface. The EDS result shows the accumulation of Cu at the large grain sites. The SEM image and EDS result validate the existence of CuO_x mixed with nearly 35% Sm oxide and 1% Ce oxide on the sur-

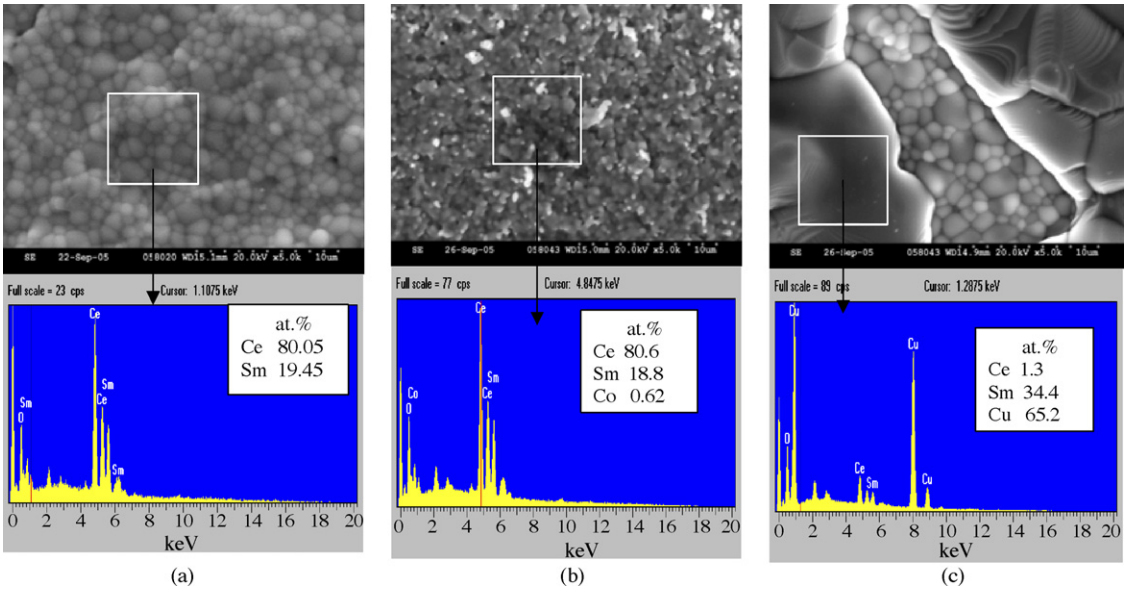

Fig. 8. SEM and EDS analysis of: (a) SDC, (b) 1%Co-SDC and (c) 1%Cu-SDC.

face of the 1%Cu-SDC samples. Other Cu-SDC samples show a similar surface morphology. After surface polishing, EDS could not detect the tenorite CuO-rich phase, indicating that the new phase was generated and accumulated at the surface layer of the sample, which was probably related to a vapour-condense formation mechanism.

3.6. Sintering mechanism of SDC with sintering aids

For pure SDC, grain boundary and volume diffusion govern the densification [16]. The linear shrinkage rate is expressed as follows

$$-\frac{\mathrm{d}L}{L\mathrm{d}t} = \frac{\gamma V_\mathrm{a}}{kT}\frac{AD_0}{G^n}\exp\left(\frac{-E_\mathrm{a}}{kT}\right) \quad (1)$$

Here, L is the actual sample length, γ the surface energy, V_a the atomic volume, A, D_0 and n are the parameters specific to the dominant diffusion mechanisms. G is the actual grain size, k the Boltzmann constant, T the experienced temperature and E_a is the apparent activation energy. For the grain boundary diffusion, $n=4$, for volume diffusion $n=3$. Provided that A and G are independent of the density, the E_a of the densification can be determined by simple plotting the $\ln(-\mathrm{d}L/L\mathrm{d}t)T$ versus $1/T$ at a constant relative density for different heating rates. In most cases G is dependent on density, the E_a of the densification can be obtained by plotting the $\ln(\mathrm{d}L/L\mathrm{d}t)TG^n$ versus $1/T$. The grain size can be obtained from the sintered body and measures as a function of relative density. In this study, the SDC grain size was not drastically increased between with (1000 °C for 5 h) and without sintering aids (1400 °C for 5 h) (see Fig. 8).

The enhanced sintering behavior of SDC with cobalt oxide sintering aid were assigned to the existence of a Co oxide rich amorphous grain boundary film by Kleinlogel and Gauckler [12], this grain boundary layer acts as fast diffusion path during the densification. A model of activated solid-state sintering has been proposed by German and Rabin [17] based on the enhanced densification rate through the formation of a grain boundary layer for the addition of small amounts of aids to a base material. Zhang et al. [18] elucidated the sintering mechanism of Fe-doped ceria with two different sintering models and found that doping with Fe introduces a viscous flow mechanism in the first stage of sintering. Jud et al. [16] studied $Gd_{0.2}$ $Ce_{0.8}O_{1.9}$ (GDC) adding 1 mol% cobalt oxide with constant heating rate dilatometry. They conclude that cobalt oxide changes the grain boundary structure of GDC resulting in enhanced mass transport and increased densification rates. While pure GDC exhibits a significant amount of surface diffusion, Co oxide doping enhances grain boundary diffusion. The sintering of Co oxide doped GDC occurs by rearrangement and grain boundary diffusion. The activation energies are 467 ± 31 and $620 \pm 31\,\mathrm{kJ\,mol^{-1}}$ for pure GDC and with 1 mol% cobalt oxide, respectively.

Meng and co-workers [19] employed Makipirtti–Meng equation for the sintering kinetics of SDC with addition of 5 mol% cobalt oxide. They found that addition of cobalt oxide enhanced the densification rate greatly by changing the sintering mechanism. The shrinkage process can be divided into three stages with different apparent activation energies. For the first stage (800–850 °C), the sintering relates to the sintering within aggregates ($E_\mathrm{a} = 66.4\,\mathrm{kJ\,mol^{-1}}$). In the second stage (900–1000 °C), it relates to accelerate the surface diffusion and grain boundary diffusion through the amorphous layer ($E_\mathrm{a} = 468\,\mathrm{kJ\,mol^{-1}}$). For the third stage (1050–1150 °C), the sintering corresponds the mass diffusion ($E_\mathrm{a} = 71.8\,\mathrm{kJ\,mol^{-1}}$). And their results are consistent to the SEM microstructure observation.

In this study, it seems that Co-SDC samples follow the above-mentioned activated solid-state sintering models [16–19]. Small grain size in the sintered Co-SDC sample suggests that most of densification is accomplished by rearrangement of grains and boundary layer diffusions. However, in Cu-SDC samples, it was clear that new phase of low melt point with composition of Cu–Sm–Ce–O_x was found and the fast densification could be due to the liquid phase diffusion under capillary action along with grains rearrangement.

4. Conclusions

Commercial micrometer-sized SDC powder could be sintered to fully density below 1000 °C by adding 1 at.% Cu or Co oxide. Sintering of Cu- or Co-SDC powder at 1000 °C gave sufficient density with limited grain growth of the original SDC powder. SDC with Cu addition shows the lowest sintering temperature and fastest sintering rate at 920 °C, which is 300 °C lower than that of the SDC powder. An impurity phase consisting of 65% Cu oxide and 35% Sm oxide was found at the surface during the densification at 1000 °C, which can be removed by surface polishing. SDC with 2.5 at.% Co shows limited impact on the SDC electrochemical properties, while reducing the sintering temperature to below 1000 °C.

Acknowledgement

This work was part of the National Solid Oxide Fuel Cell Project supported by the Canadian National Fuel Cell and Hydrogen Program. The authors would like to thank Wei Qu, Justin Roller, Yongsong Xie and Rob Hui for the experimental support.

References

[1] Z. Shao, S.M. Haile, Nature 431 (2005) 170.
[2] X. Zhang, M. Robertson, C. Decès-Petit, Y. Xie, R. Hui, S. Yick, E. Styles, J. Roller, O. Kesler, R. Maric, D. Ghosh, J. Power Sources, in press.
[3] H. Yoshida, T. Inagaki, J. Alloys Compd. 408–412 (2006) 632.
[4] J.F. Braumard, C. Gault, A. Argoitia, J. Less-Common Met. 127 (1987) 125.
[5] T. Kudo, H. Obayashi, J. Electrochem. Soc. 122 (1975) 142.
[6] H. Yahiro, K. Eguchi, H. Arai, J. Electrochem. Soc. 135 (1998) 2077.
[7] Y. Zhou, M.N. Rahaman, Acta Mater. 45 (1997) 3635.
[8] K. Yamashita, K.V. Ramanujachary, M. Greenblatt, Solid State Ionics 81 (1995) 53.
[9] J. Li, T. Ikegami, T. Mori, Acta Mater. 52 (2004) 2221.
[10] T.S. Zhang, J. Ma, Y.L.B. Kong, P. Hing, Y.J. Leng, S.H. Chan, J.A. Kilner, J. Power Sources 124 (2003) 26.
[11] D.J. Seo, K.O. Ryn, S.B. Park, K.Y. Kim, R.H. Song, Mater. Res. Bull., in press.
[12] C. Kleinlogel, L.J. Gauckler, Solid State Ionics 135 (2000) 567.

[13] T.S. Zhang, J. Ma, Y.J. Leng, S.H. Chan, P. Hing, J.A. Kilner, Solid State Ionics 168 (2004) 187.
[14] T.S. Zhang, P. Hing, H.T. Huang, J.A. Kilner, J. Eur. Ceram. Soc. 21 (2001) 221.
[15] J.S. Lee, K.H. Choi, B.K. Ryu, B.C. Shin, I.S. Kim, Ceram. Int. 30 (2004) 807.
[16] E. Jud, C.B. Huwiler, L.J. Gauckler, J. Am. Ceram. Soc. 88 (2005) 3013.
[17] R.M. German, B.H. Rabin, Powder Metall. 28 (1985) 7.
[18] T.S. Zhang, P. Hing, H.T. Huang, D.L. Johnson, J. Mater. Sci. 37 (2002) 997.
[19] R. Yan, F. Chu, Q. Ma, X. Liu, G. Meng, Mater. Lett., in press.